

Article

Numerical Investigation of the Knocking Combustion Characteristics of the N-Butanol/N-Octanol RCCI Engine

Jing Li *, Dajian Wang, Cong Zhuang, Shiqi Gong and Songhong Li

School of Mechanical and Power Engineering, Nanjing Tech University, Nanjing 211816, China

* Correspondence: jingli@njtech.edu.cn

Abstract: The n-butanol/n-octanol fueled reactivity-controlled compression ignition engine was numerically studied based on the KIVA-CHEMKIN code. First, the knocking combustion characteristics were analyzed while functioning with a premixed n-butanol percentage of 20% (B20), since it exhibited the most severe knocking. Ten local regions were monitored to obtain local data, such as pressure and heat release rate. The local pressure oscillation was quantified by a band-pass filter. Second, the premixed n-butanol percentage and the intake valve close (IVC) timing were varied to investigate their effects on the combustion characteristics and emissions formations, as well as their potential for mitigating knocking. The results showed that a strong pressure oscillation was observed for B20 near the cylinder wall, which indicates severe knocking. This consequence is mainly caused by the low-temperature combustion of the n-octanol/n-butanol/air mixture near the cylinder-wall region. Increasing premixed n-butanol percentage and retarding IVC timing could result in an extended ignition delay, lowered peak pressure, and reduced maximum pressure rise rate (PRR). Condition B80 with an IVC timing of -126° ATDC could improve the indicated mean effective pressure by 11.7% and reduce the maximum PRR by 63.4% when compared to condition B20.

Keywords: n-butanol; n-octanol; RCCI engine; knock; combustion



Citation: Li, J.; Wang, D.; Zhuang, C.; Gong, S.; Li, S. Numerical Investigation of the Knocking Combustion Characteristics of the N-Butanol/N-Octanol RCCI Engine. *Processes* **2022**, *10*, 2142. <https://doi.org/10.3390/pr10102142>

Academic Editor: Albert Ratner

Received: 30 September 2022

Accepted: 19 October 2022

Published: 20 October 2022

Publisher's Note: MDPI stays neutral with regard to jurisdictional claims in published maps and institutional affiliations.



Copyright: © 2022 by the authors. Licensee MDPI, Basel, Switzerland. This article is an open access article distributed under the terms and conditions of the Creative Commons Attribution (CC BY) license (<https://creativecommons.org/licenses/by/4.0/>).

1. Introduction

Environmental pollution and the energy crisis are two of the main reasons driving researchers to find renewable and clean energy sources and new combustion technologies. To improve the combustion efficiency and reduce the emissions of internal combustion engines (ICE), many innovative combustion strategies for ICEs have been proposed, such as homogeneous charge compression ignition (HCCI), premixed charge compression ignition (PCCI), and reactivity-controlled compression ignition (RCCI) technologies [1,2]. In particular, both HCCI and PCCI employ a single fuel, which consequently results in the disadvantage of being poorly controlled since the ignition point depends on the chemical kinetics of fuels [3,4]. In contrast, the RCCI mode, which belongs to the dual-fuel combustion mode, regulates the ratio of two fuels with different reactivity, and in conjunction with an appropriate direct injection strategy, can achieve the aim of controlling the ignition point and combustion process [5]. Hence, the RCCI mode has received widespread attention.

One of the key challenges confronting RCCI engines is the tendency of knocking under high loads [6]. Karim and Liu [7] studied the knock phenomenon in a natural gas/diesel dual-fuel engine. The results showed that the knock generally occurs during the combustion of natural gas and is more pronounced at high loads. Berenjestanaki et al. [8] suggested that the knocking phenomenon in the dual-fuel combustion mode at high loads is mainly caused by the ignition and combustion of the premixed mixture in the end gas region. To mitigate knocking, different techniques have been considered in various kinds of RCCI engines [9]. Yousefi et al. [10] studied the effect of the double injection strategy on the knocking combustion of a natural gas/diesel RCCI engine. They found that the double injection strategy could lower the speed of flame propagation which would consequently

reduce the pressure rise rate (PRR). As a result, the propensity for knocking could be lowered. Li et al. [11] simultaneously adjusted the exhaust gas recirculation (EGR) rate and intake valve close (IVC) timing to mitigate knocking with a high premixed fuel ratio. Finally, they obtained the optimal condition with significantly reduced CO, NO, and soot emissions and a marginally improved indicated mean effective pressure (IMEP).

In addition to the necessity of knocking mitigation, the demand for renewable fuels is also important for RCCI engines. The initially proposed RCCI combustion mode adopted gasoline and diesel fuels as the low- and high-reactivity fuels, respectively. Alternative fuels must be looked for from the perspectives of environmental protection and sustainable development. For example, Wang et al. [12] realized the methanol/polyoxymethylene dimethyl ethers (PODE) RCCI combustion in a high-pressure common-rail diesel engine. They found that the use of PODE with an appropriate injection strategy could help lower the PRR and extend the operating load of the RCCI engine. Sun et al. [13] chose coal to liquid (CTL) as the alternative high reactivity fuel and gasoline as the low reactivity fuel in the RCCI engine. They also compared the proposed gasoline/CTL RCCI mode with the conventional gasoline/diesel RCCI mode in terms of combustion characteristics and emissions. It was found that the use of CTL could provide more stability. Furthermore, the gasoline/CTL RCCI mode produced lower CO, HC, and soot emissions and higher thermal efficiency with optimum intake conditions, though accompanied by a slightly increased NO_x.

According to the above analysis, the proper selection of renewable fuels for the RCCI engine may also help to prevent knocking. It has been demonstrated that n-butanol performs similarly to gasoline in compression ignition engines [14]. Meanwhile, n-octanol is a perfect substitute for diesel [15,16]. Therefore, n-butanol and n-octanol can be adopted as the low- and high-reactivity fuels in RCCI engines, respectively. These alcoholic fuels have high latent heat of vaporization, which can effectively lower the combustion temperature and may help prevent knocking in RCCI engines operating under high loads. In addition, both n-butanol and n-octanol are biofuels and can be produced from lignocellulose [17]. It is known that biofuels are capable of “zero carbon emission” over a life cycle, which is consistent with China’s development objective of “carbon neutrality” [18].

In sum, the RCCI engine fueled with n-butanol and n-octanol is proposed in this study. This study aims to investigate the knocking combustion characteristics of this proposed engine by numerical means. KIVA-CHEMKIN was used to conduct the simulation. First, the models were validated by comparing the simulated results with the experimental data under various conditions. Then, the knocking combustion characteristics of the RCCI engine with 20% of premixed n-butanol were investigated with the local region analysis technique. Lastly, the effects of premixed fuel percentage and IVC timing on the combustion characteristics and emissions formation of the RCCI engine were explored.

2. Methodology

2.1. KIVA-CHEMKIN

In this study, the coupled KIVA-CHEMKIN code was used to mimic the engine combustion process [19]. In KIVA, the Kelvin-Helmholtz and Rayleigh-Taylor (KH-RT) model was used to replace the original Taylor Analogy model to provide a better prediction of the breakup process. In addition, the Re-Normalisation Group (RNG) $k-\epsilon$ model was used for turbulence calculations. However, the original KIVA version cannot deal with detailed chemistry calculations, which lowers the simulation accuracy of the combustion process of fuels. This shortcoming can be overcome by coupling CHEMKIN, which accomplishes detailed chemistry calculation. The detailed chemistry calculation for n-butanol and n-octanol can be achieved by integrating the multi-component reaction mechanism [20] developed by the authors’ group. The adopted skeletal reaction mechanism, including n-butanol and n-octanol, consists of 121 species and 623 reactions [16]. The formation process of NO_x was also embedded in this reaction mechanism. Apart from the chemical reaction mechanism of the fuels, their thermophysical properties need to be added to the

fuel library of the KIVA code. Therefore, the thermophysical properties of n-butanol and n-octanol, such as boiling point, critical properties, vapor pressure, latent heat of vaporization, density, viscosity, thermal conductivity, gas diffusion coefficient, and surface tension, were calculated based on the methods stated in reference [21]. Then the calculated data were updated in the KIVA fuel library.

2.2. Experimental Data

In this study, two types of engines were used to validate the models in the KIVA-CHEMKIN code. One is the HCCI engine fueled with neat n-butanol. The other is the conventional compression ignition (CCI) engine fueled with neat n-octanol. The experimental data of the HCCI engine and CCI engine for validation were taken from the published results reported by Han et al. [22] and Kerschgens et al. [17], respectively. Table 1 lists the specifications of the HCCI and CCI engines.

Table 1. Engine specifications [17,22].

Engine Type	HCCI Engine	CCI Engine
fuel	n-butanol	n-octanol
bore (cm)	8.6	7.5
stroke (cm)	8.6	8.83
swept volume (L)	0.499	0.39
compression ratio	18.2	15
number of spray holes	–	8
intake valve close ($^{\circ}$ ATDC)	–135	–134.6
exhaust valve open ($^{\circ}$ ATDC)	100	120

2.3. Grid Generation

Based on the information from the HCCI and CCI engines, grids were generated individually. Assuming that both geometric and flow symmetries exist in the cylinder, the sector mesh method, which could save much computational time, was adopted in this study. By conducting the grid convergence test, the average cell size of 2.0 mm was chosen [23]. Figure 1 demonstrates the generated sector meshes at the top dead-center (TDC) for the HCCI and CCI engines. It should also be noted that with the use of sector mesh, the closed-cycle simulation should be performed from the IVC timing to the exhaust valve open (EVO) timing for both engines.

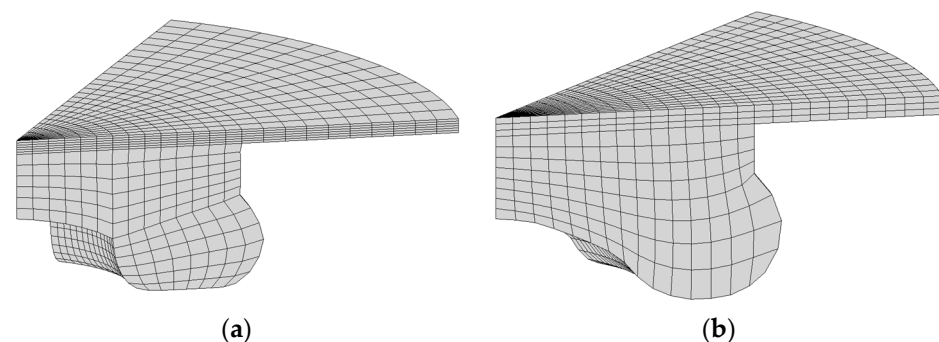


Figure 1. Generated grids at TDC: (a) HCCI engine, (b) CCI engine.

2.4. Validation

2.4.1. Validation Cases

Table 2 shows the operating conditions for the validation cases. As can be seen from the table, the n-butanol-fueled HCCI engine was operated at a speed of 1500 rpm with different EGR rates. The n-octanol-fueled CCI engine was operated at different speeds with various EGR rates.

Table 2. Operating conditions of validation cases [17,22].

Case No.	1	2	3	4
Engine type	HCCI	HCCI	CCI	CCI
Fuel type	n-butanol	n-butanol	n-octanol	n-octanol
IMEP, bar	6.5	6.5	6.8	9.4
Speed, r/min	1500	1500	1500	2280
SOI timing, °ATDC	N.A.	N.A.	−9.5	−5.3
Injection duration, °CA	N.A.	N.A.	5.5	17.4
EGR rate, %	46%	57%	47.8	43.8

The properties of n-butanol and n-octanol are given in Table 3. In comparison to n-octanol, n-butanol has a lower cetane number, which suggests that it is also less reactive. Additionally, the lower heating value of n-butanol is marginally smaller than that of n-octanol. In terms of oxygen content, the value of n-butanol is almost two times higher than that of n-octanol.

Table 3. Properties of n-butanol and n-octanol [15,24].

	N-Butanol	N-Octanol
boiling temperature, °C	118	195
density, kg/m ³	810	817
kinematic viscosity, mm ² /s (40 °C)	2.63	7.3
heat of vaporization, kJ/kg	582	562
cetane number	17–25	37
lower heating value, MJ/kg	33.21	37.6
oxygen content, wt.%	21.58	12.3

2.4.2. Validation Results

Figure 2 compares the simulated in-cylinder pressure and heat release rate (HRR) with the experimental data for both HCCI and CCI engines fueled with n-butanol and n-octanol, respectively. As is shown, the simulated in-cylinder pressure and HRR of the n-butanol fueled HCCI engine can accurately reproduce the experimental data, except that the peak HRR is marginally higher. As for the n-octanol fueled CCI engine, though the simulated ignition time is earlier than the experimental results, the discrepancies are still within an acceptable level. In summary, the models and reaction mechanism adopted in this study are reliable.

2.5. Means of Knocking Analysis

2.5.1. Local Regions Analysis

It is common to adopt mean pressure and HRR to analyze the combustion characteristics of engines. For RCCI engines, the end-gas autoignition may occur. It would be very helpful to detect the occurrence of the end-gas autoignition with the aid of the local region analysis technique. In this study, the n-butanol/n-octanol RCCI combustion was realized by premixing n-butanol in the n-octanol fueled CCI engine. That is, the RCCI combustion was modeled based on the CCI engine given in Table 1. Therefore, to realize the local analysis, ten local regions (R1–R10) were defined in the geometry of the CCI engine, as illustrated in Figure 3. Among the ten local regions, R1–R5 are located in the piston bowl area, R6–R8 are on the top of the piston crown, and R9 and R10 are near the cylinder wall. By defining the regions, information such as pressure and HRR of the local regions can be extracted for detailed analysis.

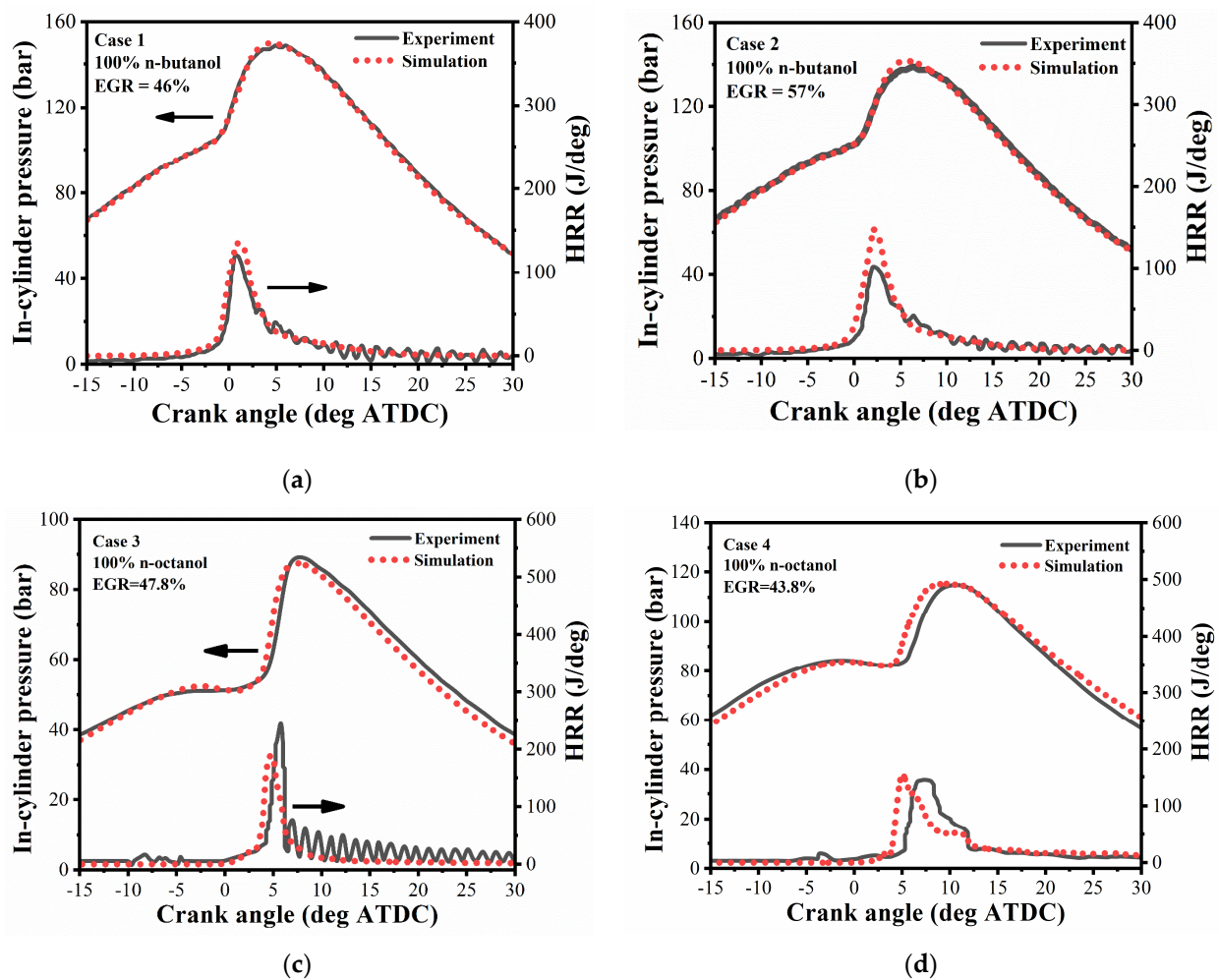


Figure 2. Validation in-cylinder pressure and HRR of HCCI and CCI engines: (a) Case 1, (b) Case 2, (c) Case 3, (d) Case 4.

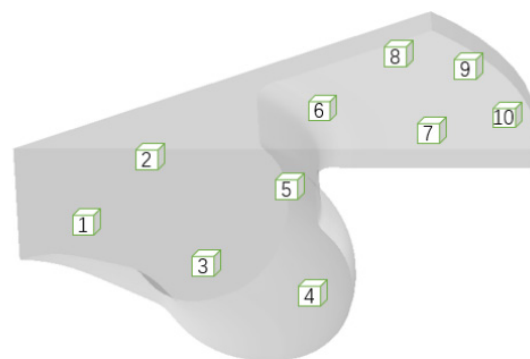


Figure 3. Distribution of the defined ten local regions (R1–R10).

2.5.2. Knocking Identification

In this study, the analysis of local in-cylinder pressure was carried out to identify the onset of knocking [25]. A fourth-order Butterworth band-pass filter was used to process the pressure data; as a result, the peak-to-peak PPmax can be obtained to quantify pressure oscillation. First, using the analytical solution of the wave equation for a closed cylinder with two flat ends, the resonant knocking frequencies were calculated to determine the Butterworth band-pass filter cut-off frequency. The resonant frequency is calculated by Equation (1).

$$f_{m,n} = \alpha_{m,n} \frac{c_s}{\pi B} \quad (1)$$

where $\alpha_{m,n}$ is the wave number determined employing Bessel's equation; m and n are the numbers of radial and circumferential pressure nodes, respectively; c_s represents the speed of sound; and B stands for the bore of a cylinder. The calculated theoretical values at different vibration modes are given in Table 4. As can be seen, when the high-cutoff and low-cutoff Butterworth filter frequencies were set to 5 kHz and 25 kHz, respectively, the main spectral components associated with knocking could be identified while maintaining a reasonable signal-to-noise ratio.

Table 4. The calculated value of resonance frequency at the temperature of 2500 K.

Resonance Frequency	f_{10}	f_{20}	f_{01}	f_{30}	f_{40}	f_{11}
theoretical value (kHz)	7.04	11.67	14.65	16.06	20.33	20.38
vibration mode	 1,0	 2,0	 0,1	 3,0	 4,0	 1,1

2.6. Study Cases

Based on validation condition 4, the EGR rate was changed to 0%, and the percentage of n-butanol varied from 0% to 90%. According to the n-butanol percentage, the corresponding working conditions are designated as B0 to B90. When varying the premixed n-butanol percentage, the total energy input was kept constant. The premixed n-butanol percentage can be determined by Equation (2):

$$\text{Premixed fuel percentage} = \frac{M_{but} LHV_{but}}{M_{oct} LHV_{oct} + M_{but} LHV_{but}} \quad (2)$$

where M_{but} means the mass of n-butanol (kg); M_{oct} means the mass of n-octanol (kg); LHV_{but} means the lower heating value of n-butanol (MJ/kg); and LHV_{oct} means the lower heating value of n-octanol (MJ/kg). Besides premixing n-butanol, the start of injection (SOI) timing was advanced to -20° ATDC to realize the RCCI combustion. Then, knocking combustion characteristics were investigated under the B20 condition. At last, the potential of varying premixed fuel percentage and IVC timing on knocking mitigation was examined.

3. Results and Discussion

3.1. Characteristics of Knocking Combustion

3.1.1. Local Pressure

The local pressures in the ten regions of the cylinder were acquired through simulation. The Butterworth Filter was employed to quantify pressure oscillation, and the local maximum pressure PPmax was then determined in different regions; the region with the most tendency of knocking can then be determined. Figure 4 shows the pressure and its local PPmax for the ten regions under B20 working conditions. As can be seen from the graph, the in-cylinder pressure curves of the R2–R6 regions are relatively smooth. Fluctuations in the process of pressure rising become obvious in R1 and R7–R10. Furthermore, fluctuations become stronger in regions R9 and R10, which indicates that the knocking tends to happen in the vicinity of the cylinder wall.

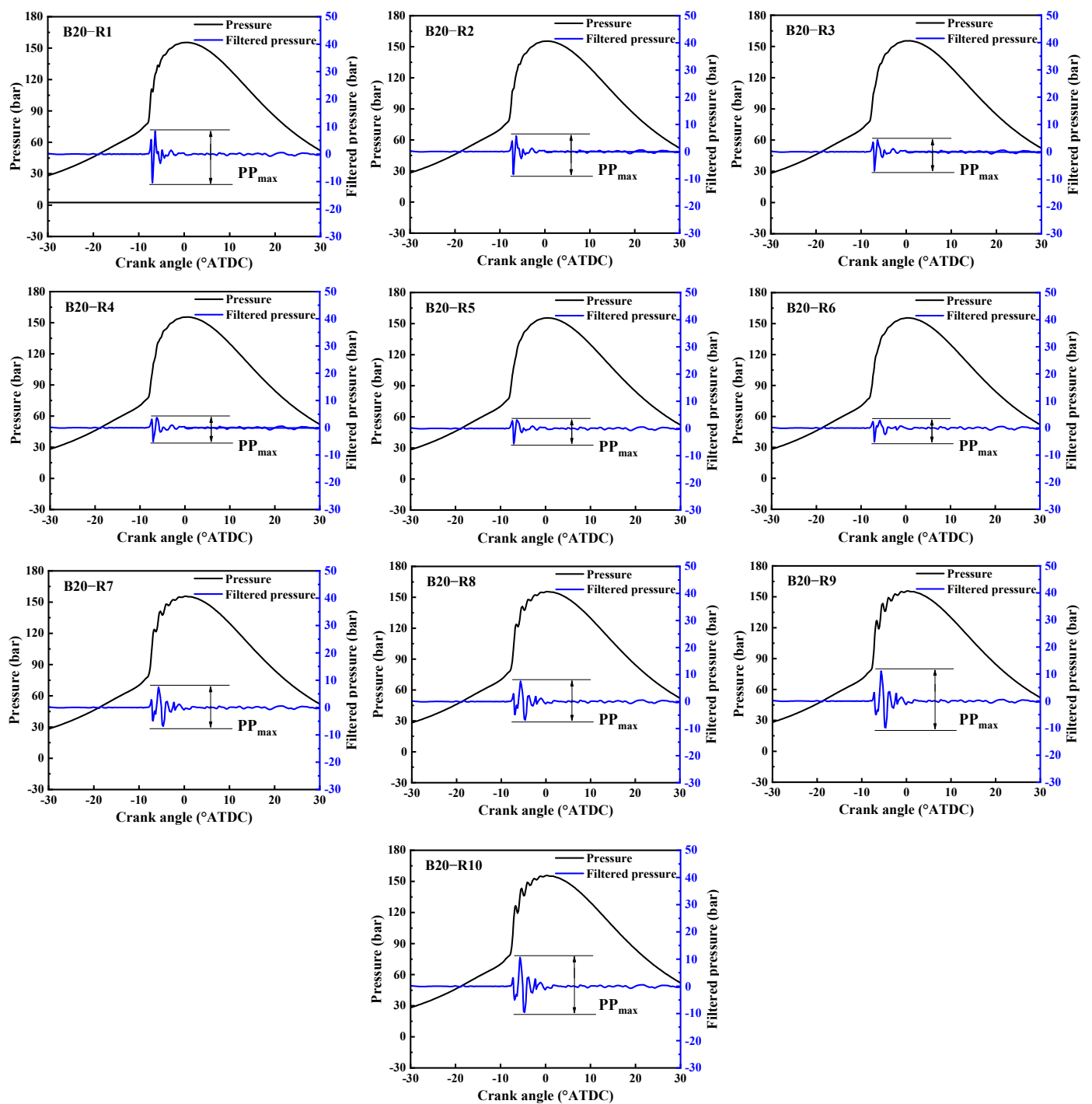


Figure 4. Comparison of local in-cylinder pressure and maximum pressure PP_{max} in regions R1–R10 under B20 working conditions.

Figure 5 compares the PP_{max} of the ten regions under B20 working conditions. When PP_{max} is less than 10 bar, the engine is considered to be under normal combustion conditions [26]. Therefore, regions R3–R6 exhibit normal combustion. R1, R2, R7 and R8 regions show a moderate knocking phenomenon. Noticeably, severe knocking is produced in the vicinity of the cylinder wall (R9 and R10), since an obvious pressure oscillation phenomenon is observed.

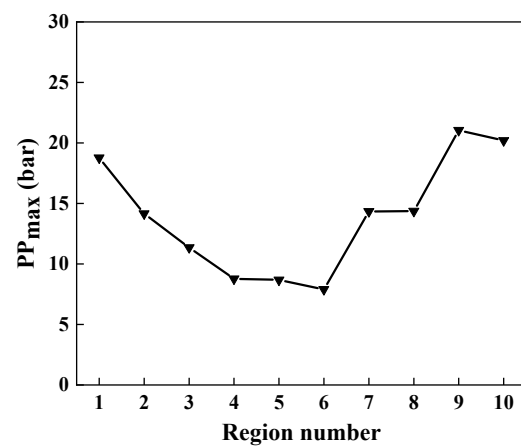


Figure 5. Comparison of PPmax in all ten regions under B20 working conditions.

3.1.2. Temperature and Radical Concentration Analysis

Analyzing the concentration of radicals is an effective method to determine whether auto-ignition occurs in the end gas. In this study, OH concentration and ROOH concentration are used as the basis for high-temperature and low-temperature combustion evaluation, respectively. Figure 6 compares the spatial distribution of temperature, OH and ROOH concentrations at different crank angles for the B20 condition.

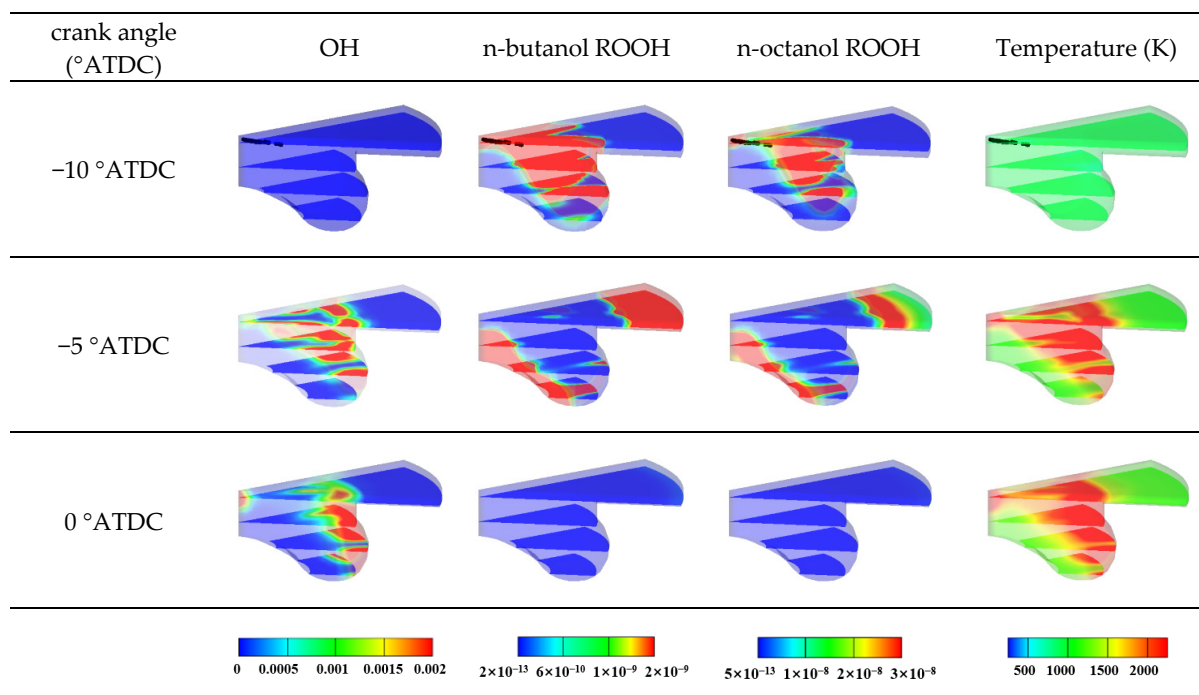


Figure 6. Comparison of the concentration distribution of OH, ROOH, and temperature under B20 working condition.

When the crank angle is -10° ATDC, the in-cylinder temperature is around 1000 K. At this moment, OH radicals have not yet been generated; however, ROOH radicals associated with n-butanol and n-octanol, respectively, have been generated in the bowl region of the combustion chamber. This result indicates that low-temperature combustion occurs in the bowl region of the combustion chamber at this moment. This is attributed to the injection of n-octanol into the combustion chamber bowl region. In more detail: n-octanol is injected into the n-butanol/air mixture, and fuel spray and mixing processes occur, followed by the low-temperature combustion of both fuels.

When the crank angle is -5° ATDC, the temperature in the bowl region can reach more than 2000 K. At this time, the ROOH radicals generated by the two fuels in the bowl region have been completely consumed, while a large amount of OH radicals have also been generated. This indicates that high-temperature combustion occurs in the bowl region of the cylinder at this time. Simultaneously, a considerable amount of n-octanol ROOH and n-butanol ROOH are produced adjacent to the cylinder wall and the centerline of the combustion chamber, implying that low-temperature combustion occurs in these regions. This reveals that the low-temperature combustion of n-octanol and n-butanol starts from the bowl region and then gradually propagates to the two sides, that is, there are two development directions: one is “from bowl to centerline”, and the other is “from bowl to cylinder wall”. When the piston reaches the TDC, the ROOH radicals are completely consumed, and the OH radicals are still mainly distributed in the vicinity of the bowl region. The temperature distribution also indicates that high-temperature combustion is mostly concentrated in the bowl region, and it is not observed in the vicinity of the cylinder wall.

From the pressure oscillation curves in the R9 and R10 regions in Figure 4, it can be seen that the more intense pressure oscillation produced in the vicinity of the cylinder wall also occurs at the crank angle of -5° ATDC, which is consistent with the moment when low-temperature combustion of n-octanol and n-butanol occurs in the vicinity of the cylinder wall. Therefore, it can be inferred that the severe knocking in the vicinity of the cylinder wall is caused by the low-temperature combustion of the fuels.

3.1.3. Local HRR

Figure 7 demonstrates the total HRR and local HRR of the ten regions. It can be seen that the total HRR curve starts to rise around -13° ATDC and reaches a peak at around -8° ATDC. In conjunction with the analysis of Figure 6, it is clear that the heat generated before -10° ATDC originates from the low-temperature combustion of n-butanol and n-octanol in the bowl region of the combustion chamber.

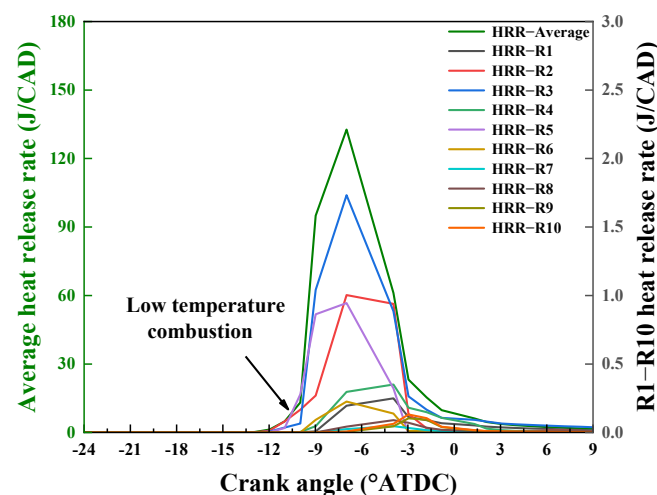


Figure 7. Comparison of the average in-cylinder heat release rate and local heat release rate of the ten regions under B20 working conditions.

Furthermore, the heat generated from regions R2, R3, and R5 is also substantially higher than that from the other regions after -8° ATDC. This result indicates that the high-temperature combustion occurs in the bowl area of the combustion chamber and generates a large amount of heat. This phenomenon is consistent with the temperature distribution shown in Figure 6, i.e., the region where more heat is released is at a higher temperature. However, the peak heat release rate is lower near the cylinder wall (R7–R10). Based on the analysis in Section 3.1.2, it can be inferred that the relatively small amount of heat released comes mainly from the regions near the cylinder wall and near the centerline of the combustion chamber where the low-temperature combustion happens.

3.1.4. Local PRR

Figure 8 compares the PRR of the ten regions under B20 working conditions. As shown in the figure, when the crank angle is -8° ATDC, the peak PRR is relatively lower in the region adjacent to the cylinder wall (R9 and R10). In contrast, the highest peak PRR occurs in the bowl area of the combustion chamber. This would be mainly due to the high-temperature combustion occurring in the bowl area and the low-temperature combustion occurring near the cylinder wall. However, there is a further sharp increase in the PRR at the region near the cylinder wall (R9 and R10) at the crank angle of roughly -5° ATDC. This crank angle coincides with the presence of a large amount of n-butanol ROOH and n-octanol ROOH in the region near the cylinder wall, as illustrated in Figure 6. Therefore, it can be inferred that the high PRR around the crank angle of -5° ATDC is caused by the occurrence of low-temperature combustion of the fuels.

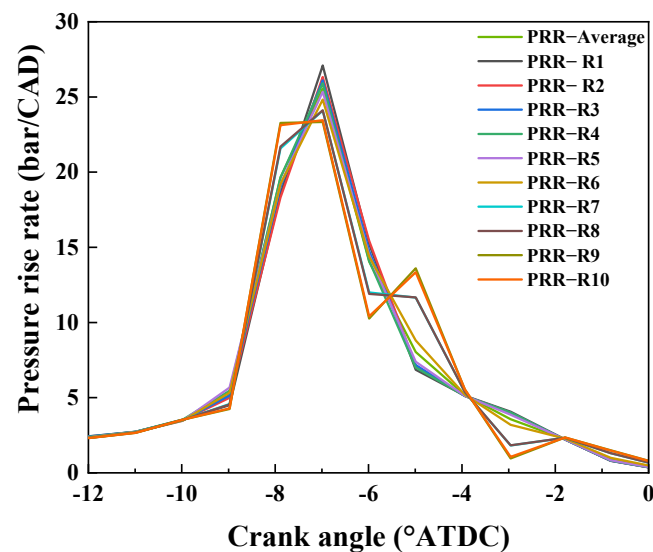


Figure 8. Pressure rise rate of the ten regions under B20 working conditions.

In addition, R9 and R10 display higher PPmax compared with other regions (Figure 5), and the pressure curves of R9 and R10 exhibit significant pressure oscillation around -5° ATDC (Figure 4). Hence, it can also be inferred that the high PPmax in the region near the cylinder wall is caused by the low-temperature combustion occurring in the end gas region where the combustion of n-octanol/n-butanol/air mixture occurs.

3.2. Effects of Premixed Fuel Percentage

In this section, the combustion characteristics and emissions formation are analyzed by varying the percentage of n-butanol from 0% to 90%.

3.2.1. In-Cylinder Pressure and HRR

Figure 9 shows the comparison of in-cylinder pressure and HRR with different premixed n-butanol percentages. As can be seen from the in-cylinder profiles, the increased n-butanol percentage leads to an increased ignition delay. For B10 to B50, the ignition points are all relatively close to each other, which implies that the effect of fuel percentage on the ignition delay is small under these conditions. However, when the premixed percentage of n-butanol is increased to 60% and above, a significant impact on the ignition delay can be observed. Especially for the B90 condition, the ignition point has been retarded after the TDC. This is mainly associated with the reactivity of the fuels. As is known, the reactivity of n-butanol is lower than that of n-octanol. Therefore, the global reactivity in the dual-fuel engine would be reduced by increasing the premixed percentage of n-butanol. Consequently, the ignition point gradually moves backward as more n-butanol is premixed.

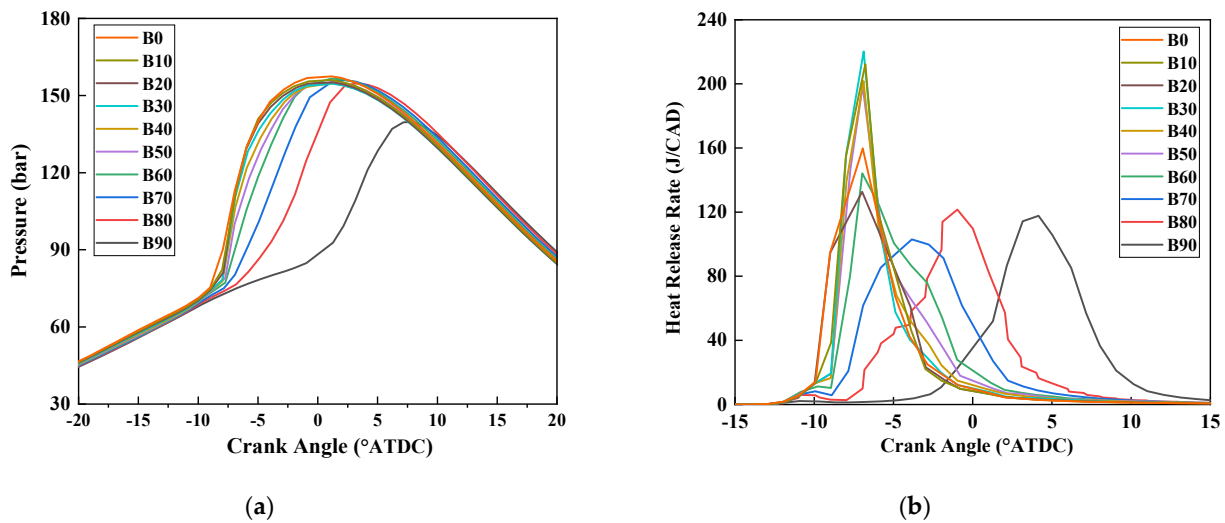


Figure 9. Comparison of in-cylinder pressure and HRR under different n-octanol percentages: (a) in-cylinder pressure, (b) HRR.

It can be observed from the HRR curves that increasing the premixed n-butanol could slow the HRR and extend the combustion duration. Meanwhile, the peak HRR first increases and then decreases, and its position gradually shifts backward. This phenomenon is primarily caused by the interaction of the fuel oxygen content and the in-cylinder reactivity gradient. It is known that n-butanol contains more oxygen than n-octanol does. The higher the n-butanol percentage, the higher the oxygen content of the fuel mixture in the cylinder, which benefits the combustion process. As a result, the peak HRR is initially increased gradually for the conditions of B10 to B40.

3.2.2. Maximum PRR

Figure 10 compares the maximum PRR for various n-butanol percentages. As can be seen from the graph, as the percentage of n-butanol increases, the maximum PRR increases and then decreases. The trend of maximum PRR correlates with the HRR. The higher the peak HRR, the faster the pressure rises. It is known that the PRR is an indicator of engine knock. The threshold is 10 bar/degree. Therefore, all the working conditions explored in this study experienced the knock phenomenon, with B20 experiencing the most intense knocking. It should also be noted that this result is inconsistent with one of a gasoline/biodiesel RCCI engine discussed in the literature [27]. Li et al. found that premixing more gasoline resulted in a higher maximum PRR [27], whereas, in this study, premixing more n-butanol was beneficial in reducing the PRR. This may be due to the lower reactivity of n-butanol compared to gasoline.

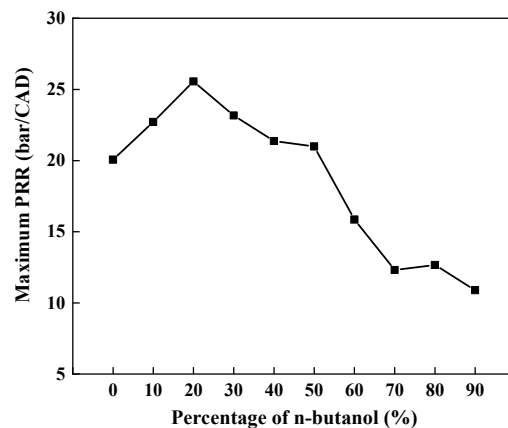


Figure 10. Comparison of maximum pressure rise rate under different n-butanol percentages.

3.2.3. Temperature Distribution

Figure 11 shows the simulated evolution of spatial temperature (K) distributions under conditions of B20 and B80. The figure shows that B20 starts high-temperature combustion at -5° ATDC, and the high-temperature combustion area is widely distributed. In contrast, B80 is currently just starting to ignite, and the combustion initiation is in the bowl-shaped area. From 5° to 15° ATDC, B80 has fewer areas with a high temperature ($T > 2200$ K) in the cylinder than B20, but it has a higher temperature close to the cylinder wall. This implies that the temperature distribution of B80 is more homogeneous. At 20° ATDC, the in-cylinder temperature of B80 is below 2000 K, while the B20 still shows some areas with a temperature above 2000 K, indicating a shorter combustion duration of B80.

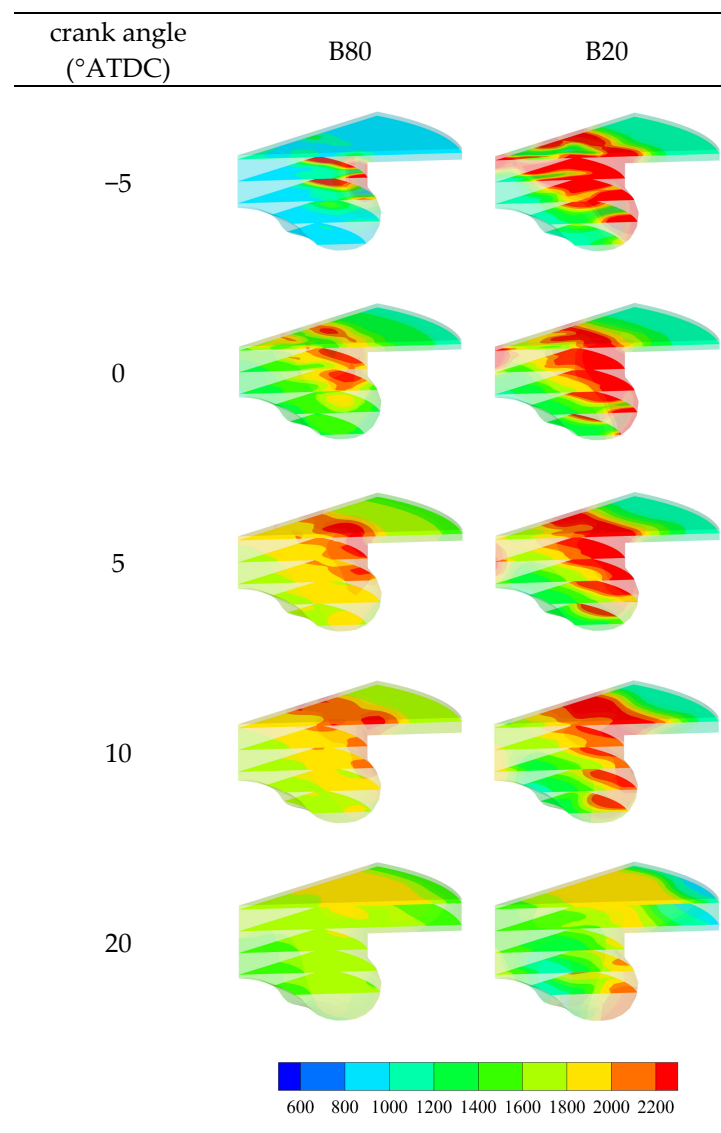


Figure 11. Simulated evolution of spatial temperature (K) distributions under conditions of B20 and B80.

3.2.4. IMEP

Figure 12 compares the IMEP for various n-butanol percentages. As can be seen, with the increase in n-butanol percentage, IMEP shows a trend of first decreasing and then increasing. The maximum IMEP is observed for B90. It can also be found that the IMEPs of B0~B50 are between $8.5\sim 9.0$ bar. This can be implied from the in-cylinder pressure curves. As is demonstrated in Figure 9, the pressure curves of B0~B50 do not differ much;

in addition, their start of combustion timings are all before TDC, which makes the engine work less efficient. In contrast, the IMEP is significantly improved when the percentage of n-butanol is raised to more than 60%. This is mainly due to the longer ignition delay for these conditions. As a result, the start of combustion timing is closer to the TDC, which is advantageous for the efficient operation of the engine.

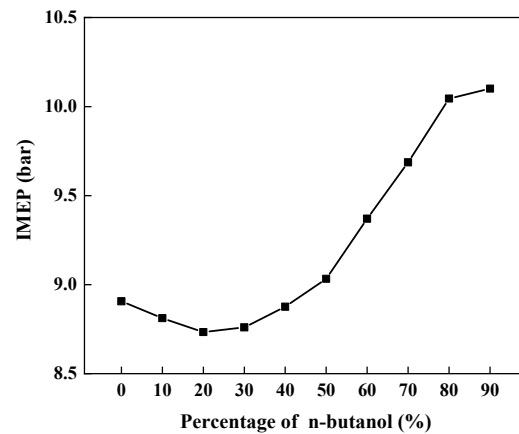


Figure 12. IMEP with different n-butanol percentages.

3.2.5. Emissions

Figure 13 compares the NO_x and CO emissions with different n-butanol percentages. As can be observed, with the increase of n-butanol percentage, NO_x emission is significantly reduced. This is because a high percentage of premixed n-butanol leads to a longer ignition delay period. Therefore, the fuel and air have sufficient mixing time and can achieve low-temperature combustion.

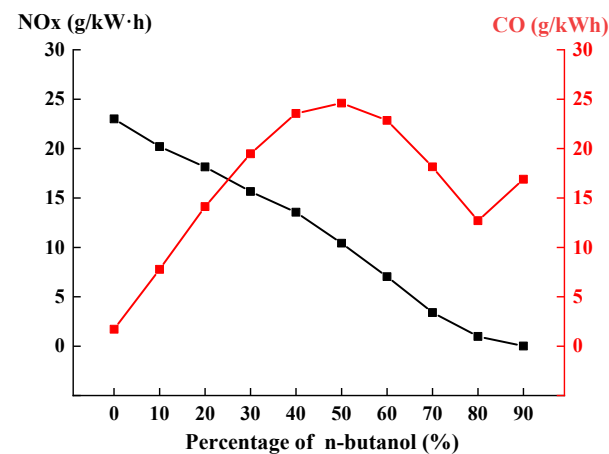


Figure 13. NO_x and CO emissions with different n-butanol percentages.

As for CO emission, a first increasing and then decreasing trend can be seen as more n-butanol is premixed. Figure 14 demonstrates the spatial distribution of CO under conditions of B20 and B80. Due to the premixed n-butanol, CO is formed in the region near the cylinder wall. What's more, B80 produces much more CO near the cylinder wall. However, the CO of B80 is eventually oxidized due to a higher combustion temperature near the cylinder wall (Figure 11). Another reason is that the oxygen content of n-butanol is higher than that of n-octanol, leading to better oxidation of CO when premixing more n-butanol.

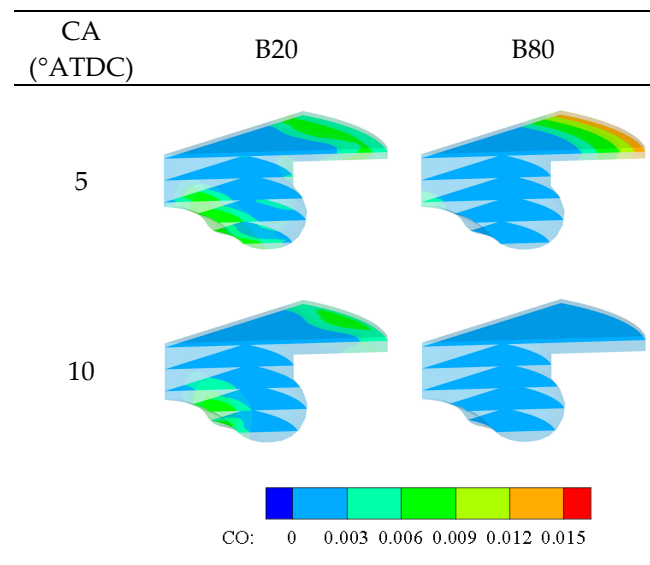


Figure 14. Simulated evolution of spatial CO distributions under conditions of B20 and B80.

In summary, B80 can achieve high IMEP with low NO_x and CO emissions. The maximum PRR is marginally higher than the critical value (10 bar/degree). Hence, B80 is selected as the benchmark for the following study on the effects of IVC timing.

3.3. Effects of IVC Timing

In this section, the combustion characteristics and emissions formation are analyzed with the IVC timings of -134 , -130 , -126 , -122 , and -118 °ATDC.

3.3.1. In-Cylinder Pressure and HRR

Figure 15 illustrates the comparison of in-cylinder pressure and HRR with different IVC timings. It can be observed that retarding IVC timing could lead to a longer ignition delay and a lower peak pressure. The main reason is that retarding IVC timing reduces the effective compression ratio and is not favorable for ignition. In addition, the reduced effective compression ratio can lower the back pressure of the cylinder, which is not beneficial to the air-fuel mixing process.

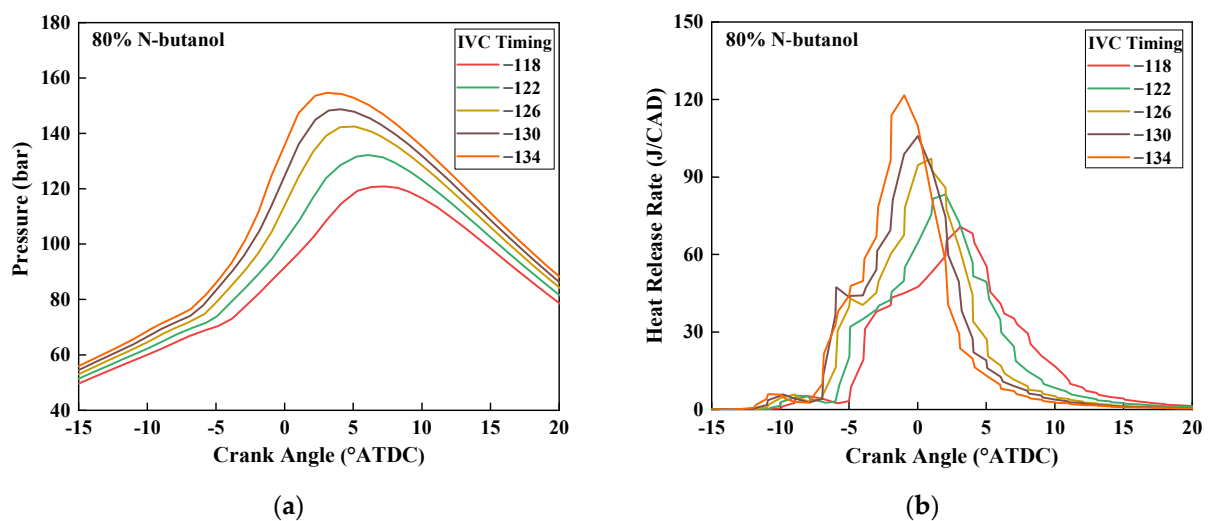


Figure 15. Comparison of in-cylinder pressure and HRR under different IVC timings: (a) in-cylinder pressure, (b) HRR.

From HRR curves, two-stage combustion, including low-temperature and high-temperature combustion stages, can be observed for the n-butanol/n-octanol RCCI engine. This low-temperature stage combustion, around -10° ATDC, is caused by the negative temperature coefficient behavior of n-octanol [28]. Another phenomenon that can be seen is that the peak HRR decreases with the delay of the IVC timing. This result is correlated with the phenomenon observed in the cylinder pressure curve. This is also mainly caused by the decrease in the effective compression ratio.

3.3.2. Maximum PRR

Figure 16 shows the maximum PRR of the RCCI engine with various IVC timings. As can be seen, the maximum PRR decreases significantly with the delay of IVC timing, showing a linear relationship. Hence, it can be inferred that reducing the effective compression ratio is a promising method for mitigating the knocking phenomenon of the dual-fuel engine. When the IVC timing is retarded after -126° ATDC, the maximum PRR could be reduced below 10 bar/degree, which can mitigate the knocking phenomenon.

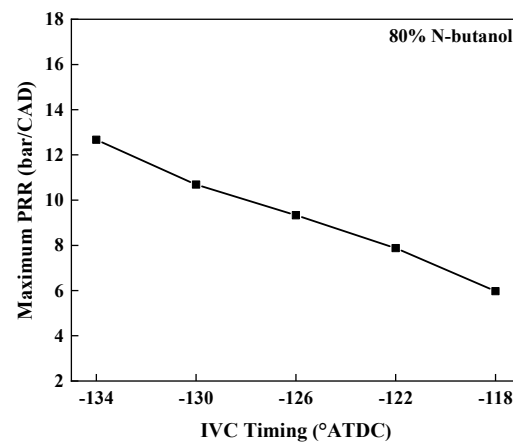


Figure 16. Comparison of maximum PRR under different IVC timings.

3.3.3. Temperature

Figure 17 displays the simulated evolution of spatial temperature (K) distributions under conditions with IVC timings of -134° and -118° ATDC. With the IVC timing of -134° ATDC, high-temperature combustion regions already appear at -5° ATDC. At the TDC, the temperature reaches more than 1000 K at all locations in the cylinder. As for the IVC timing of -118° ATDC, the high-temperature combustion regions only appear around the TDC. Meanwhile, the temperature at the bowl region is always lower than that with IVC timing of -134° ATDC. This phenomenon is consistent with the results for in-cylinder pressure and HRR, mainly because the IVC timing of -118° ATDC has a low effective compression ratio, which is not beneficial for high-temperature combustion.

3.3.4. IMEP

Figure 18 compares the IMEP for various IVC timings. As retarding the IVC timing, IMEP shows a trend of decreasing, which correlates with the trend of maximum PRR. As discussed, retarding the IVC timing will decrease the effective compression ratio, which consequently deteriorates the thermal efficiency of the engine. Therefore, the IMEP is reduced with the delayed IVC timing. However, it should be noted that the condition with IVC timing of -126° ATDC shows an IMEP of 9.7 bar with an acceptable maximum PRR, which is still higher than that of the B20 case discussed in Section 3.2.4.

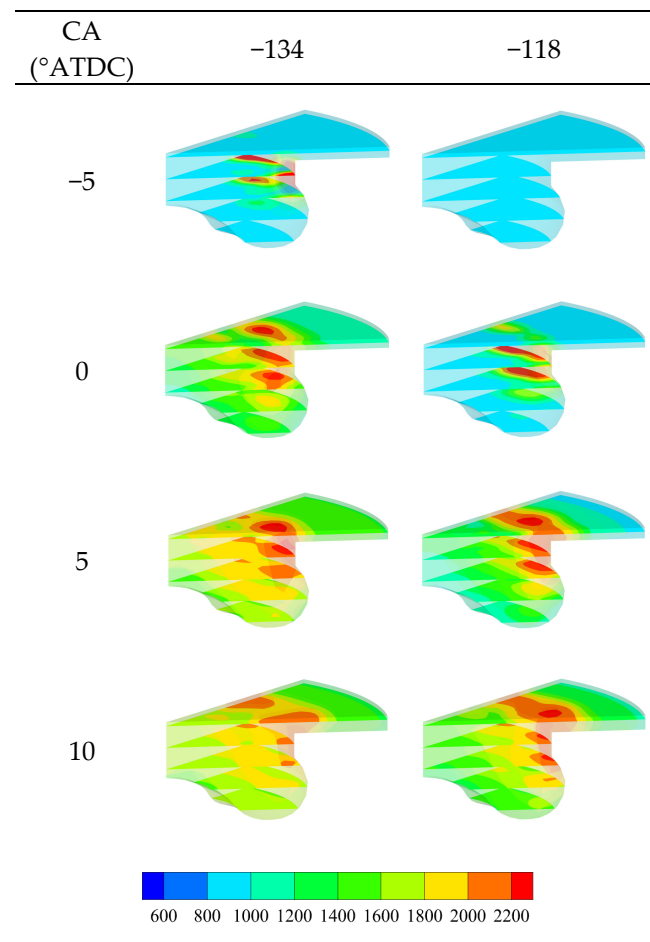


Figure 17. Simulated evolution of spatial temperature (K) distributions under conditions of IVC timings of -134° and -118° ATDC.

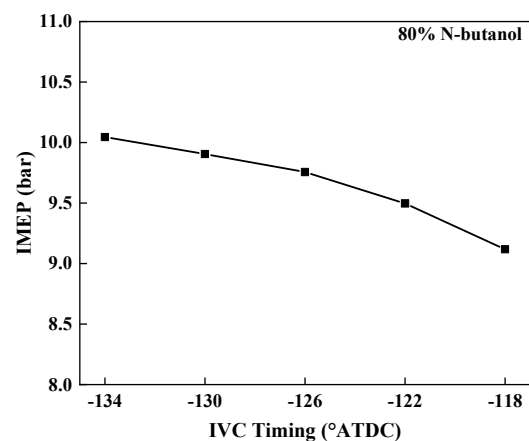


Figure 18. IMEP for various IVC timings.

3.3.5. Emissions

Figure 19 compares the NO_x and CO emissions with different IVC timings. It is found that with the delay of IVC timing, NO_x emission is significantly reduced. This is because retarding IVC timing will lead to a decrease in the combustion temperature, as discussed in Section 3.3.3. At the same time, the duration of high-temperature combustion is also reduced with the delayed IVC timing. As a result, less NO_x is formed.

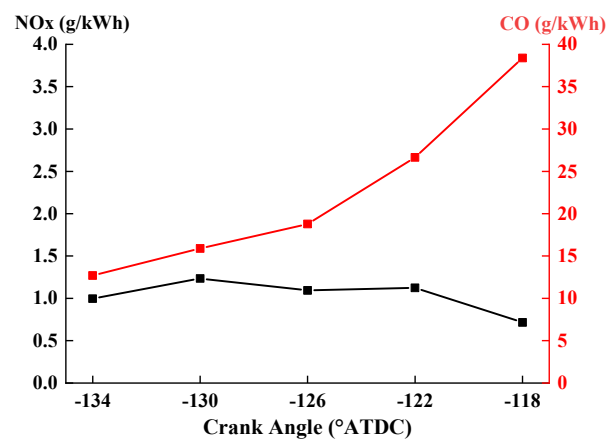


Figure 19. NOx and CO emissions with different IVC timings.

A different trend is observed for CO emission. When retarding the IVC timing, the CO emission shows a trend of increasing, which demonstrates a negative correlation with the maximum PRR and IMEP. Figure 20 demonstrates the spatial distribution of CO under conditions with IVC timings of -134° and -118° ATDC. As can be seen from the figure, when the IVC timing is -118° ATDC, a large amount of CO is formed in the bowl region of the combustion chamber and the CO near the centerline of the combustion chamber is not completely oxidized after generation. This is mainly because the temperature in the region near the centerline of the cylinder is low, as illustrated in Figure 17. As a result, the generated CO cannot be fully oxidized. In comparison, in the condition with IVC timing of -134° ATDC, the CO generated in the bowl region is generally able to be oxidized.

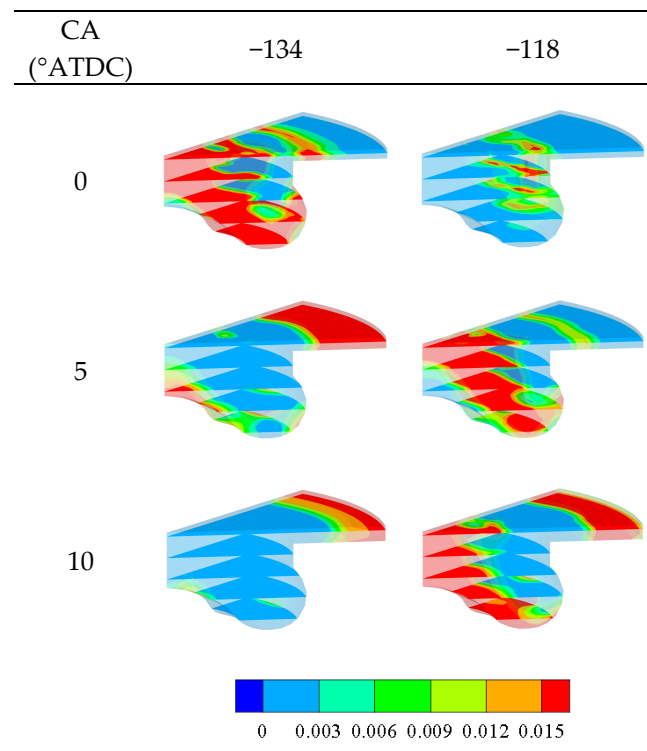


Figure 20. Simulated evolution of spatial CO distributions under conditions with IVC timings of -134° and -118° ATDC.

4. Conclusions

In this study, the combustion characteristics of the n-butanol/n-octanol RCCI engine were investigated by the numerical tool KIVA-CHEMKIN. First, to comprehensively understand the characteristics of knocking combustion, local pressure was obtained by monitoring ten local regions and was processed by a fourth-order Butterworth band-pass filter to quantify the pressure oscillation. In addition, the analysis of local HRR, local maximum PRR, and radical concentrations was carried out to reveal the knocking combustion characteristics. Second, the premixed fuel percentage and IVC timing were varied to see their effects on global in-cylinder pressure, HRR, maximum PRR, IMEP, and emissions. Major conclusions are drawn as follows:

1. The B20 condition exhibited the most intense knocking. Early in the combustion process, low-temperature combustion of n-octanol and n-butanol started in the bowl area, moving gradually in two directions to the centerline and cylinder wall. Additionally, the low-temperature combustion of the n-octanol/n-butanol/air mixture produced the most pronounced pressure oscillation closest to the engine cylinder wall.
2. Generally, increasing the premixed n-butanol percentage resulted in an extended ignition delay, lowered peak pressure, and reduced maximum PRR. Meanwhile, continuing to increase the premixed fuel percentage beyond 50% would increase IMEP while decreasing CO and NO_x simultaneously. This result indicates that the selection of n-butanol as a premixed fuel is more competitive than gasoline.
3. Retarding the IVC timing could also prolong the ignition delay, lower the peak pressure, decrease the maximum PRR, and deteriorate the IMEP. In addition, the CO emissions could be raised, but the NO_x emissions decreased slightly.
4. Compared with condition B20, which experiences the most intense knocking, the condition with a high premixed percentage (B80) and an IVC timing of -126° ATDC could improve IMEP by 11.7% and decrease the maximum PRR by 63.4% for the engine.

Author Contributions: Conceptualization, J.L. and D.W.; Formal analysis, J.L. and D.W.; Funding acquisition, J.L.; Investigation, D.W., C.Z., S.G. and S.L.; Methodology, J.L. and D.W.; Project administration, J.L.; Resources, J.L.; Software, D.W.; Supervision, J.L.; Validation, D.W. and C.Z.; Writing—original draft, J.L. and D.W.; Writing—review & editing, J.L. and S.G. All authors have read and agreed to the published version of the manuscript.

Funding: This research was funded by the National Natural Science Foundation of China (grant number 51806098), the Natural Science Foundation of Jiangsu Province (grant number BK20171016), and the Innovation Engineering Project of Jiangsu Province (grant number SJCX22_0430).

Institutional Review Board Statement: Not applicable.

Informed Consent Statement: Not applicable.

Data Availability Statement: All data used to support the findings of this study are included within the article.

Conflicts of Interest: The authors declare no conflict of interest.

References

1. Niklawy, W.; Shahin, M.; Amin, M.I.; Elmaihy, A. Comprehensive analysis of combustion phasing of multi-injection HCCI diesel engine at different speeds and loads. *Fuel* **2022**, *314*, 123083. [[CrossRef](#)]
2. Agarwal, A.K.; Singh, A.P.; Kumar, V. Particulate characteristics of low-temperature combustion (PCCI and RCCI) strategies in single cylinder research engine for developing sustainable and cleaner transportation solution. *Environ. Pollut.* **2021**, *284*, 117375. [[CrossRef](#)] [[PubMed](#)]
3. Dimitrova, I.D.; Megaritis, T.; Ganippa, L.C.; Tingas, E.-A. Computational analysis of an HCCI engine fuelled with hydrogen/hydrogen peroxide blends. *Int. J. Hydrogen Energy* **2022**, *47*, 10083–10096. [[CrossRef](#)]
4. Lu, Y.; Fan, C.; Liu, Y.; Pei, Y. Effects of speed extension on PCCI combustion and emissions in a heavy-duty diesel engine at medium load. *Fuel* **2022**, *313*, 123048. [[CrossRef](#)]
5. Li, J.; Yang, W.; Zhou, D. Review on the management of RCCI engines. *Renew. Sustain. Energy Rev.* **2017**, *69*, 65–79. [[CrossRef](#)]

6. Zhou, W.; Xi, H.; Zhou, S.; Zhang, Z.; Shreka, M. Numerical study on knock characteristics and mechanism of a heavy duty natural gas/diesel RCCI engine. *Int. J. Hydrogen Energy* **2022**. [[CrossRef](#)]
7. Karim, G.; Liu, Z. *A Predictive Model for Knock in Dual Fuel Engines*; SAE Technical Paper 921550; SAE International: Warrendale, PA, USA, 1992.
8. Valipour Berenjestanaki, A.; Kawahara, N.; Tsuboi, K.; Tomita, E. End-gas autoignition characteristics of PREMIER combustion in a pilot fuel-ignited dual-fuel biogas engine. *Fuel* **2019**, *254*, 115634. [[CrossRef](#)]
9. Yıldız, M.; Çeper, B.A. A comparative study on gasoline/diesel-fueled RCCI combustion at different premixed ratios and high-EGR diesel CI combustion in an IC engine under low load conditions. *Fuel* **2022**, *324*, 124596. [[CrossRef](#)]
10. Yousefi, A.; Guo, H.; Birouk, M. Split diesel injection effect on knocking of natural gas/diesel dual-fuel engine at high load conditions. *Appl. Energy* **2020**, *279*, 115828. [[CrossRef](#)]
11. Li, J.; Yu, X.; Xie, J.; Yang, W. Mitigation of high pressure rise rate by varying IVC timing and EGR rate in an RCCI engine with high premixed fuel ratio. *Energy* **2020**, *192*, 116659. [[CrossRef](#)]
12. Wang, L.; Liu, J.; Ji, Q.; Sun, P.; Li, J.; Wei, M.; Liu, S. Experimental study on the high load extension of PODE/methanol RCCI combustion mode with optimized injection strategy. *Fuel* **2022**, *314*, 122726. [[CrossRef](#)]
13. Sun, W.; Zeng, W.; Guo, L.; Zhang, H.; Yan, Y.; Lin, S.; Zhu, G.; Sun, Y. Experimental investigation into the effects of pilot fuel and intake condition on combustion and emission characteristics of RCCI engine. *Fuel* **2022**, *325*, 124912. [[CrossRef](#)]
14. Chen, Z.; He, J.; Chen, H.; Geng, L.; Zhang, P. Comparative study on the combustion and emissions of dual-fuel common rail engines fueled with diesel/methanol, diesel/ethanol, and diesel/n-butanol. *Fuel* **2021**, *304*, 121360. [[CrossRef](#)]
15. García, A.; Monsalve-Serrano, J.; Villalta, D.; Zubel, M.; Pischinger, S. Potential of 1-octanol and di-n-butyl ether (DNBE) to improve the performance and reduce the emissions of a direct injected compression ignition diesel engine. *Energy Convers. Manag.* **2018**, *177*, 563–571. [[CrossRef](#)]
16. Li, J.; Liang, Y.; Yang, W. Combustion characteristics and emissions formation of a compression ignition engine fueled with C8 biofuels blends. *Energy Sources Part A Recovery Util. Environ. Eff.* **2022**, *44*, 5991–6008. [[CrossRef](#)]
17. Kerschgens, B.; Cai, L.; Pitsch, H.; Heuser, B.; Pischinger, S. Di-n-buthylether, n-octanol, and n-octane as fuel candidates for diesel engine combustion. *Combust. Flame* **2016**, *163*, 66–78. [[CrossRef](#)]
18. Zhao, X.; Ma, X.; Chen, B.; Shang, Y.; Song, M. Challenges toward carbon neutrality in China: Strategies and countermeasures. *Resour. Conserv. Recycl.* **2022**, *176*, 105959. [[CrossRef](#)]
19. Maghbouli, A.; Yang, W.; An, H.; Li, J.; Chou, S.K.; Chua, K.J. An advanced combustion model coupled with detailed chemical reaction mechanism for D.I diesel engine simulation. *Appl. Energy* **2013**, *111*, 758–770. [[CrossRef](#)]
20. Li, J.; Zhou, D.; Yang, W. A multi-component reaction mechanism of n-butanol, n-octanol, and di-n-buthylether for engine combustion. *Fuel* **2020**, *275*, 117975. [[CrossRef](#)]
21. Daubert, T.E. Physical and Thermodynamic Properties of Pure Chemicals: Data Compilation. In *Design Institute for Physical Property Data (DIPPR)*; CRC Press: Boca Raton, FL, USA, 1989.
22. Han, X.; Zheng, M.; Tjong, J.; Li, T. *Suitability Study of n-Butanol for Enabling PCCI and HCCI and RCCI Combustion on a High Compression-Ratio Diesel Engine*; SAE Technical Paper 2015-01-1807; SAE International: Warrendale, PA, USA, 2015.
23. Wang, D.; Yu, X.; Li, J.; Yang, W. Effects of combustion chamber shapes on combustion and emission characteristics for the n-octanol fueled compression ignition engine. *J. Energy Eng.* **2022**, *148*, 04022011. [[CrossRef](#)]
24. Zhang, T.; Nilsson, L.J.; Björkholtz, C.; Munch, K.; Denbratt, I. Effect of using butanol and octanol isomers on engine performance of steady state and cold start ability in different types of Diesel engines. *Fuel* **2016**, *184*, 708–717. [[CrossRef](#)]
25. Zhou, D.Z.; Yang, W.M.; An, H.; Li, J. Application of CFD-chemical kinetics approach in detecting RCCI engine knocking fuelled with biodiesel/methanol. *Appl. Energy* **2015**, *145*, 255–264. [[CrossRef](#)]
26. Long, L.; Reitz, R.D.; Iyer, C.O.; Yi, J.W. *Modeling Knock in Spark-Ignition Engines Using a G-equation Combustion Model Incorporating Detailed Chemical Kinetics*; SAE Technical Paper 2007-01-0165; SAE International: Warrendale, PA, USA, 2007.
27. Li, J.; Yang, W.; An, H.; Zhao, D. Effects of fuel ratio and injection timing on gasoline/biodiesel fueled RCCI engine: A modeling study. *Appl. Energy* **2015**, *155*, 59–67. [[CrossRef](#)]
28. Cai, L.; Uygun, Y.; Togbé, C.; Pitsch, H.; Olivier, H.; Dagaut, P.; Sarathy, S.M. An experimental and modeling study of n-octanol combustion. *Proc. Combust. Inst.* **2015**, *35*, 419–427. [[CrossRef](#)]